Scientific Research Publishing

Journal of Modern Physics, 2021, 12, 1012-1026
https://www.scirp.org/journal/jmp
ISSN Online: 2153-120X
ISSN Print: 2153-1196

Quasicrystals' Resonant Response with Translational Symmetry

Antony J. Bourdillon

UHRL, San Jose, CA, USA
Email: bourdillona@sbcglobal.net

How to cite this paper: Bourdillon, A.J. (2021) Quasicrystals' Resonant Response with Translational Symmetry. *Journal of Modern Physics*, **12**, 1012-1026.
https://doi.org/10.4236/jmp.2021.127063

Received: April 14, 2021
Accepted: May 22, 2021
Published: May 25, 2021

Abstract

Diffraction in quasicrystals is in logarithmic order and icosahedral point group symmetry. Neither of these features are allowed in Bragg diffraction, so a special theory is required. The present work displays exact agreement between the analytic metric with a numeric description of diffraction in quasicrystals that is based on quasi-structure factors. So far, we treated the hierarchic structure as ideal; now, we detail the theory by including two significant features: firstly, the steady state wave function of the incident radiation demonstrates how harmonics, in metrical space and time, enable coherent interaction between the periodic wave packet and hierarchic quasicrystal; secondly, mapping of the hierarchic structure for any influence of defects will allow estimation of possible error margins in the analysis. The hierarchic structure has the required logarithmic periodicity: superclusters, containing about 10^3 atoms, convincingly map phase contrast images; while higher orders leave space for subsidiary speculation. The diffraction is completely explained for the first time.

Keywords

Quasicrystal, Icosahedra, Hierarchic, Integral, Periodic, Resonant Response, Harmonic, Irrational, Geometric Series, Metric

1. Introducing Harmonics in Hierarchy

"Metallic phase with long range order and no translational symmetry" [1], how come? The diffraction pattern is in geometric series, is irrational, aperiodic and anharmonic. This cannot happen by Bragg's law; however, a metric results from a separable irrational part of the indices [2] [3]. This metric commensurates the periodic incident radiation with the irrational and geometric indexation that is due to the hierarchic geometry. We have previously shown how the diffraction

occurs with a lattice parameter a that is measured, analyzed, verified, complete and fundamentally classical. This novel diffraction contrasts with Bragg's law in crystals, where the order is integral, periodic, and harmonic.

In Quasicrystals, the irrational diffraction is simulated by two independent routes: one numeric by Quasi-Structure Factors (QSFs) [4]; the second derived analytically from the irrational indexation. The two independent results match exactly. Illustrations of harmonization in quasi-Bloch waves, as below, explain the metrication and coherent scattering in geometric-series, *i.e.* scattering from the irrational quasi-lattice. Knowing the ideal model and understanding the diffraction, we are now able to turn to atomic mapping, and to defects.

As a consequence of thermodynamics, all crystals are defective. The hierarchic icosahedra (HI) constitute a special case for two reasons: firstly, as Pauling noted [5], icosahedra are known in crystalline systems with large unit cells, but they include central holes. These are problematic when the cells are of regular size. Nevertheless, they are now systematically analyzed and we can fairly understand the conformability of common defects to the ideal hierarchic structure. Secondly, quasicrystals (QCs) are often rapidly quenched, so that plural defects are easily frozen into the structure. We need to investigate how they are accommodated without causing the diffraction to become diffuse owing to disorder.

The digitization and harmonization are found present in the scattered radiation during its diffractive interaction with the geometric quasi-lattice. Quasi-Bloch waves, in the resonant response of the probe, commensurate and harmonize in scattering. Their behavior resembles quantum transitions of the harmonic wave functions used in time-independent atomic physics. Both processes are consequences of wave-particle duality that is the crowning result of 19th century physics. The diffraction is mediated by the wave-packet, that will be briefly reviewed to illustrate harmonization.

Notice that our main literature review is given in ref. [1]. The present work is unique in its derivation of complete diffraction, by conventional description, in 4-dimensions, and with a systematic and extensible model that is perfectly hierarchic; perfectly icosahedral; and in perfect geometric series[1], like the diffraction.

2. Scattering Radiation

Digitization and harmony are discovered in the scattered wave, so we need to review generally the nature of radiant scatterers in the broader scope of physics. The Michelson-Morley experiment falsified the ether hypothesis. An attempt was made to salvage it with the Lorentz transformation, but this was not as successful as Einstein's foundational relativity. That "physical laws are invariant in all inertial reference systems", has been verified in many ways. A consequence is the Pythagorean style equation for rest mass: $m_0^2c^4 = E^2 - p^2c^2$. After quantization by Planck's law for energy E, and the de Broglie hypothesis for momentum p, and with simplification of units $\hbar = c = 1$ for the reduced Planck constant

[1]Further descriptions can be found in recent listings in http://www.xraylithography.com.

$\hbar$ and the speed of light c, the rest mass reduces to:

$$m_0^2 = \omega^2 - k^2 = (\omega + k)(\omega - k). \quad (1)$$

The brackets symbolize in turn *particulate* conservation laws and response that is *wave-like*, resonant and harmonic. The former is real; the latter imaginary. The particle-wave duality is thus formulated in respective real and imaginary parts of the *normal wave packet* [6]:

$$\varphi = A \cdot \exp\left(\frac{X^2}{2\sigma^2} + X\right)$$

with imaginary:

$$X = i(\bar{\omega}t - \bar{k}x) \quad (2)$$

where σ depends on initial conditions, and describes the coherence of the packet in space and time[2]; and A^2 is a normalizing constant[3]. The angular frequencies ω and wave vectors k are in fact distributed, but they are represented in equation 1 by mean values. The intensity $\phi^*\phi$ is a probability density function for a particle, or for a photon having zero mass, $m_0 = 0$. Notice that the response is elastic because its absolute, measurable value is unity: $(e^X)^* e^X = 1$, everywhere and at all time.

Incidentally, a profound solution for Equation (1) has negative mass. This implies, by the first order derivation $E = m'c^2$ with $m' = m_0\left(1 - v_g^2/c^2\right)^{-1/2}$, that $\omega < 0$ and $k < 0$. These implications are supported by the facts that $(\omega < 0 \cup k > 0) \supset$ singularities in ω and k when $|m_0| = |k|$. The singularities are not observed (*cf.* [7]); whereas, by contrast, the phase velocity $v_p = \omega/k > 0$ and group velocity $v_g = k/m' = \mathrm{d}\omega/\mathrm{d}k > 0$ are always positive [6] (cf. the Switching Principle [8] [9]).

Meanwhile, Equation (2) represents the steady state for the incident radiation and, after a transition involving a change in vector k, it represents, likewise, the steady state of the diffracted wave. When the incident wave strikes the QC, it interacts with the QC field to form quasi-Bloch waves. You can think of these as lattice images observed in thin foils in the two-beam condition. The waves, as they proceed through the QC, oscillate (by the pendellösung effect) between the two beams (in crystals: [10]; *cf.* in QCs: [11] [2]). In wedge specimens, this oscillation produces images of 'thickness fringes'. The process requires and ensures harmonic interaction, in both space and time, in the propagation direction as in the transverse. An example will be given in the next section, though the 'quasi-lattice image' will not be a true lattice image[4] because of the metric.

Notice that Equations (2) linearize the second order Equation (1) of special relativity, and so they perform a similar function for the free particle as Dirac's

[2]Typically, the coherence has transverse components, σ_y, σ_z as well, but these are only implied here for simplicity.

[3]Typically, $A^*A = m_0^2 \Big/ \int \exp\left(X^2/\sigma^2\right)\mathrm{d}\tau$.

[4]Because of the metrical displacement (except at geometric intercepts) of the quasi-Bloch wave from the quasi-lattice. This will be illustrated below.

equation does for the bound electronic states in an atom. Moreover, the equations 2 separate the propagation direction from the transverse direction, and this has many consequences including: solutions for negative mass [12][5], phase velocity [6], uncertainty, Newton's second law, electron spin, magnetic radius and fine structure constant [13][6], reduction of the wave packet [14] etc. The equations apply in harmonious diffraction by quasicrystals and crystals, as they do in the Schrödinger equation that operates on steady-state, harmonic bases. The diffraction orders and quantum numbers respectively describe interaction requirements that are quantized by *necessary constructive interference over space and time.* Equation (2) describes the fundamental radiant packet that gives required information about the structure of quasicrystals. The formalism enables our understanding of the fundamental interaction required in the coherent diffraction.

3. Properties of Hierarchic Icosahedra

The quasicrystal responds to incident radiation with sharp, icosahedral diffraction that is in irrational and geometric order. The diffraction must be long range because sharp. The principal axes are indexed in 3-dimensions (**Figure 1**) and so is the diffraction pattern [4]. However, phase-contrast imaging contradicts the classic order because it is anharmonic owing to multiple, aperiodic, interplanar spacings. It emerges that the quasicrystal is hierarchically ordered and uniquely icosahedral, with dense unit cells that are bound within icosahedral clusters. The hierarchy is infinitely extensible. There is translational symmetry: it is in the radiant quasi-Bloch-waves that are excited by the quasi-Bragg condition so as to commensurate with the aperiodic ordering. In doing so, the waves harmonize and digitize the hierarchic quasi-lattice. These functions are numerically and analytically derived, so that the quasi-lattice is measured and consistently verified. Harmony is essential to the digitized interaction as it is in quantum basis state solutions to Schrödinger's equation.

It will become clear how the structure is hierarchic and therefore geometric. The scattering radiation is periodic (Equation (2)), but is excited by the geometric quasi-lattice, to form hierarchically commensurate quasi-Bloch-waves. Corresponding periodic excitations are routinely analyzed in crystals [10], but are now adapted for QCs [15] [11]. In **Figure 2(b)** a crystalline Bloch wave (blue) is compared with a corresponding quasi-Bloch-wave (red wave) that metrically stretches the blue wave by the inverse coherence factor $1/c_s$. This is calculated both numerically and analytically [2]. Whereas the crystalline Bloch wave is not commensurate with the geometric, irrational and logarithmically-periodic quasi-lattice; the quasi-Bloch-wave is commensurate with the geometric and hierarchic

[5]To avoid unphysical singularities when $k = -m_0$ in the antiparticle, the switching principle is switched back [6].

[6]Dirac used a rank 8 matrix [Pais A, in Paul Dirac, the man and his work, ed. Goddard, P., *Cambridge* (1998) ISBN 0521583829] to calculate the fine structure constant; the approximate answer by dispersion dynamics is the same but given in rank 2 [13].

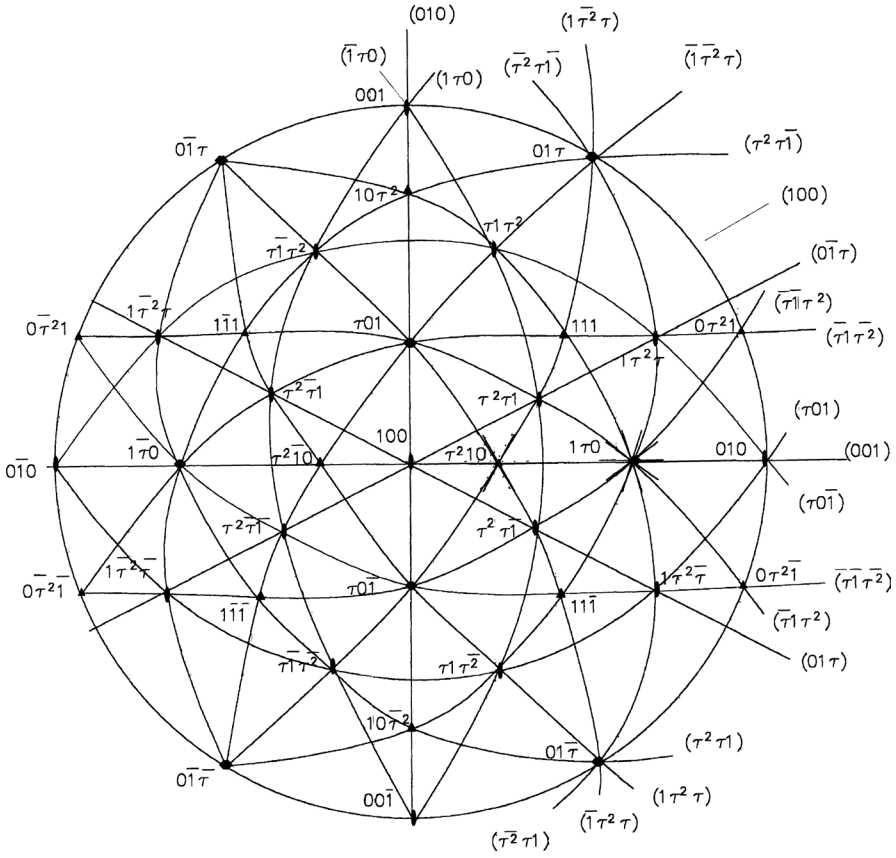

Figure 1. Stereogram of the principal axes for the icosahedral structure. Normal to them are the principal diffraction planes. They are all 3-dimensional with indices τ^m where the golden section $\tau = \left(1+\sqrt{5}\right)/2$. After William of Ockham, "Dimensions should not be multiplied without necessity." All of the beam intensities in the original data [1] have been indexed and calculated [16].

structure, and is invariant about all translations $a\tau^m$. This translational symmetry opposes Shechtman's claim [1]. The harmonization is obtained through the Fibonacci series digitization of periodic cycles between geometric intercepts (Equation (3) below). The harmonization is both long-range and local around each intercept.

So long as we understand how the diffraction occurs, there is no need to decide whether 'hierarchic symmetry' should be called 'translational'. Principal features of the complex structure and diffraction of hierarchic icosahedra justify the following summary:

Summary:

- The point group symmetry is icosahedral, in the diffraction pattern, consistent with the structure [1].
- The pattern is sharp [1].
- The orders are in geometric series [4] [16] [17].
- The series are irrational. They do not therefore obey Bragg's law for crystal diffraction [4] [16] [17].

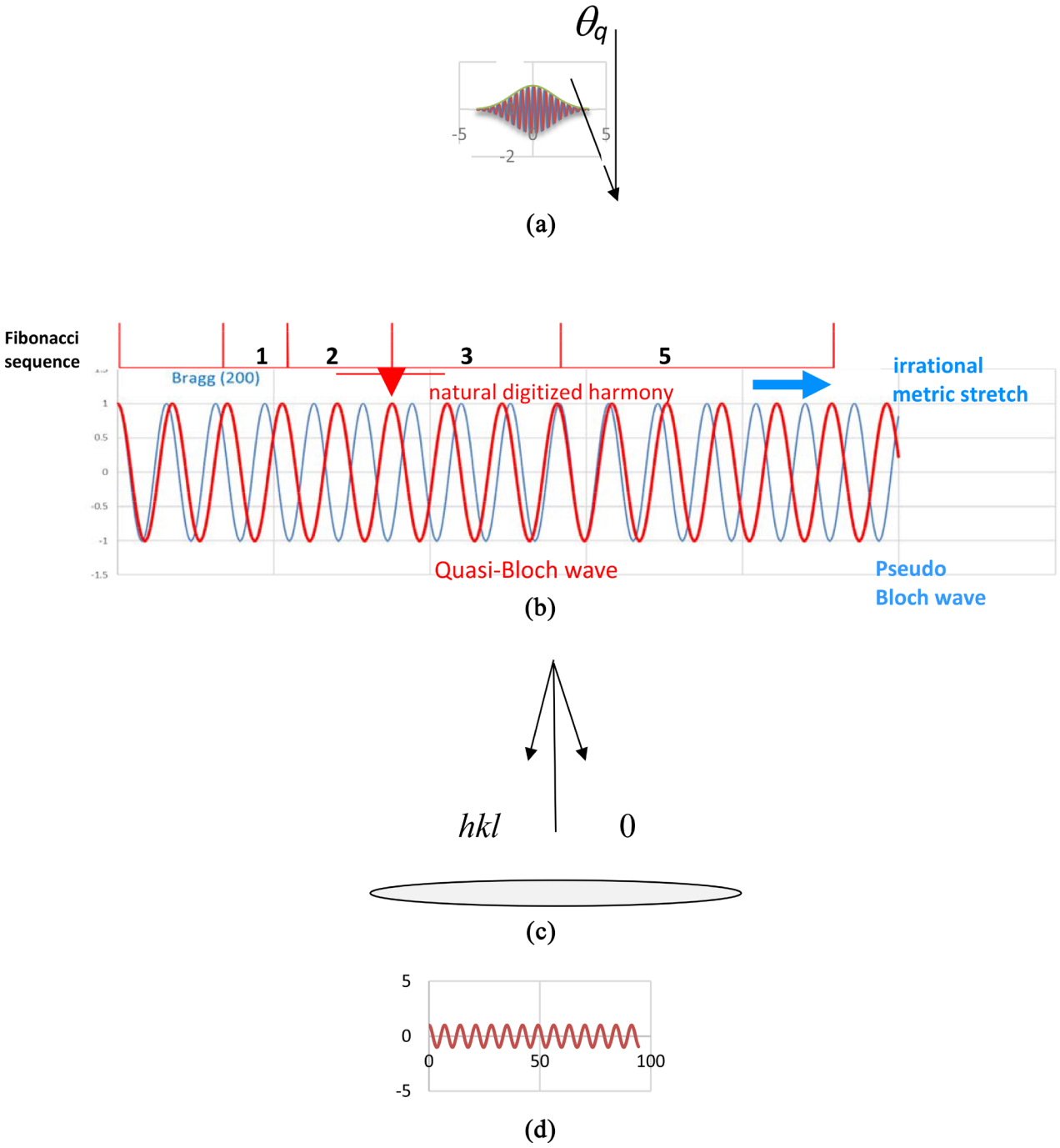

Figure 2. (a) Incident, time-dependent, beam probe (Equation (2)), rank $\Re^4$, inclined at quasi-Bragg angle from normal: $\theta_q = \sin^{-1}\left(\lambda\sqrt{h^2+k^2+l^2}\right)\Big/\left(2ac_s\right)$. (b) Crystalline Bloch waves (blue) are commensurate with their corresponding periodic crystal lattice at the Bragg condition. When this wave is stretched horizontally by the inverse coherence factor $1/c_s$, the quasi-Bloch-wave (QBW in red) commensurates with the irrational, geometric and hierarchic, quasi-lattice. Its geometric order is represented by the intercepts on the horizontal line above it [17] [16]. The digitized number of periodic cycles between successive intercepts is in Fibonacci sequence (denominator in Equation (3)), and the diffraction is logarithmically periodic. The natural and irrational parts of the indices are separable: the irrational part is expressed by the metric stretch; the natural part scatters with sharp, coherent diffraction. (c) Diffracted beams emitted beneath foil, including indices. (d) In a transmission electron microscope, beams can be magnetically refocused to produce a quasi-lattice image of the *probe* at the base of the specimen foil. The lattice image is the interference due to the superposition.

- The stereogram and planar indexations are 3-dimensional (**Figure 1** [18]). "Dimensions should not be multiplied without necessity".
  But, inclusion of time for harmony *is* necessary: the rank is $\Re^4$.
- All structure factors under Bragg's law are zero. The Quasi-Structure-Factor contains a numerical metric c_s that is peculiar to the icosahedral hierarchy, and that is calculated iteratively over successive orders of cluster and super cluster[7]: the formulaic function of the metric is a virtual breathing strain [4] [16] [17], cohering with hierarchy.
- Quasi-structure-factors map intensities in experimental diffraction patterns [4] [16] [17].
- Indices $\tau^m = F_m(1,\tau) = \partial_{(m,1)} + F_{m+1}(0,1) + F_m(0,1)\tau$ where the Fibonacci sequences F_m (0, 1) are of natural numbers on bases 0, 1 [2]. The metric is analyzed by separating the irrational parts of the indices [2] [3].
- The metric function is given by the irrational residue in the formula [2]:

$$\frac{1}{c_s} = 1 + \frac{\tau^m - F_{m+4}/2}{F_{m+1}} = \frac{1}{0.894} \tag{3}$$

- Diffraction, on the irrational indices, metricates, digitizes and harmonizes the geometric series (**Figure 2**) [2].
- These features are necessities for radiation scattering by coherent diffraction [2].
- The quasi-lattice-parameter a is measured, analyzed, harmonized, verified and complete [2J
- The dense unit cell is consistent with the fact that diatomic QCs occur only with the atomic diameter ratio: $d_{\text{solute}}/d_{\text{solvent}} = \sqrt{1+\tau^2} - 1$ [4] [16] [17]
- Phase contrast optimum defocus images in thin specimens [19] display clear hierarchies (containing ~10^3 atoms), with dimensions that match corresponding hierarchic structures that are simulated. The hierarchic structure is infinitely extensible [4] [16] [17] (present work).

4. Mapping Simulations of Phase Contrast Images

Figure 3 illustrates the extremely dense unit cell. At its center is the small *Mn* atom with its comparatively large atomic scattering factor, surrounded by 12 tightly packed *Al* atoms. The ratio of atomic diameters is $d_{\text{Mn}}/d_{\text{Al}} = \sqrt{1+t^2} - 1$. Notice the 5-fold axis that is normal to two circles of 5 *Al* atoms. This structure will prove significant in images and maps: when two planes are imaged together, they adopt the appearance of 10-fold rotational symmetry; but when imaged alone in sufficiently thin specimens, the plane appears 5-fold.

[7]The QSF F^P for a supercluster order p, with Miller indices h, k, l, is equal to the QSF order p-1 multiplied by the function for the phase due to the stretching factor τ^{2P}, where $\boldsymbol{h}$ is the corresponding normal vector for the (hkl) plane; c_s the metric; and $\boldsymbol{r}$ the vector representing the position of either an atomic site in the unit cell, or the center in a subcluster [2]:

$$F_{hkl}^{p} = \sum_{i=1}^{\text{all atoms}} \cos\left(2\pi \cdot c_s\left(\overline{h_{hkl}} \cdot \tau^{2p}\overline{r_{cc}}\right)\right) \cdot F_{hkl}^{p-1}$$

The unit cell is edge sharing, not face sharing as in crystals. The stoichiometry is therefore Al_6Mn.

In Figure 4 the unit cells are hierarchically arranged within clusters. Notice that the unit edge width of the icosahedral unit cell stretches to τ^2 in the icosahedral cluster. The hierarchy extends infinitely to superconductors order p with stretching factors τ^{2p} compared to the cluster.

The atoms illustrated in Figure 3 and Figure 4 were localized on Cartesian axes as was first done to calculate structure factors [4] [16]. The 5-fold [1 τ0] axis was identified and the position (x_0,y_0,z_0) of each atom in a quasicrystal of selected size (superclusters orders 1 and 2 in figure 5a). These atoms were all projected onto the (1 τ0) plane at points (x_2,y_2,z_2) using rotation formulae the about z axis:

$$\begin{aligned} y_2 &= \left(y_0 - x_0 t\right) \Big/ \left(1+t^2\right), \\ x_2 &= \left(x_0 t^2 - y_0 t\right) \Big/ \left(1+t^2\right), \text{and } z_2 = z_0 \end{aligned} \tag{4}$$

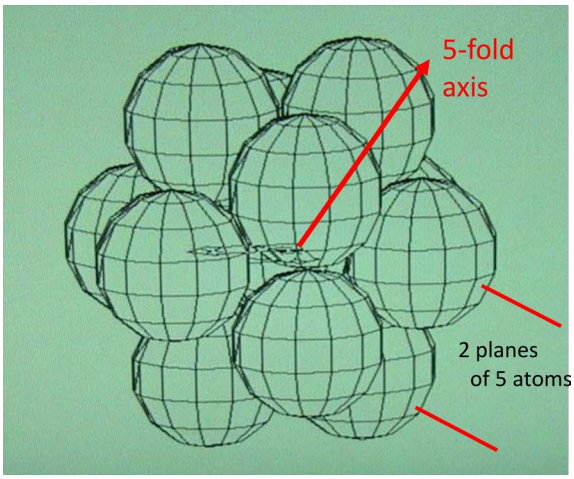

Figure 3. Extremely dense icosahedral unit cell. At its center is the small *Mn* atom with its comparatively large atomic scattering factor, surrounded by twelve tightly packed *Al* atoms.

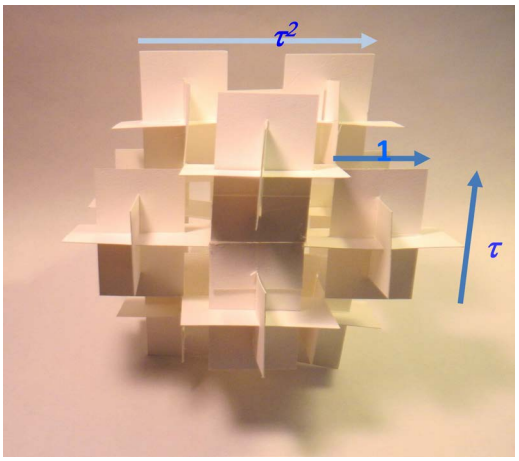

Figure 4. Hierarchy of icosahedral unit cells in the icosahedral cluster. The stretching factor is τ^2. The structure is infinitely extensible. The triad of golden rectangles can represent any member of the hierarchic series.

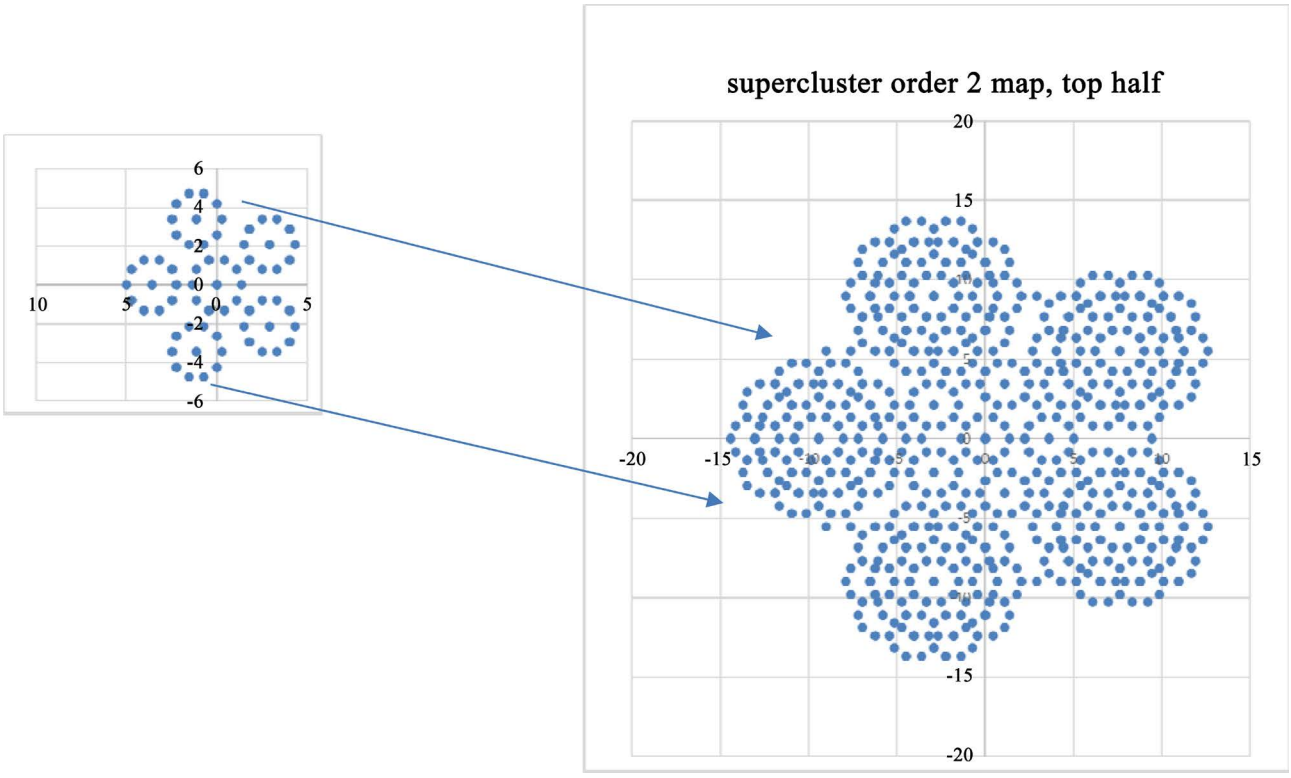

(a)

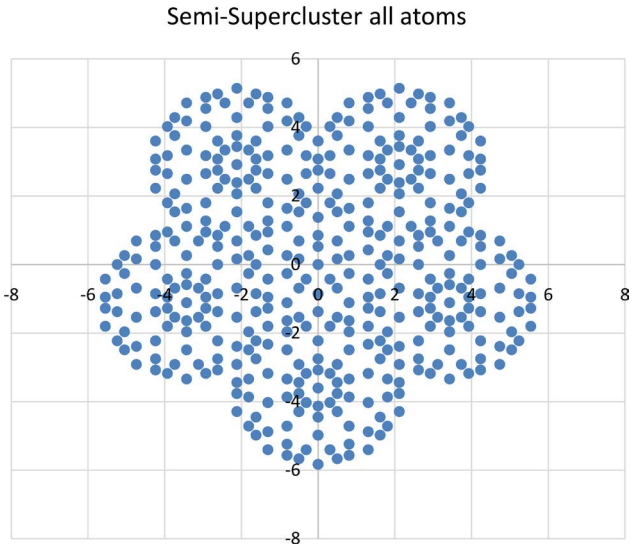

(b)

Figure 5. (a) At left is a map of *Mn* atoms in a semi-supercluster (cluster in **Figure 4** scaled up by τ^2), simulating phase-contrast images from foils ~2 nm thick owing to the large atomic scattering factor of *Mn*. Two planes of unit cells (**Figure 3** & **Figure 4**) map as a circle of 10 unit cells within a single circle of 5 clusters. These structures are experimentally evident in **Figure 6** [19]. At right, the semi-supercluster order 2 (scaled up by τ^4) would be ~5 nm thick. The full supercluster map would appear to have 10-fold symmetry, though individual second order superclusters are not distinguishable in imaging, because they overlap neighboring superclusters. (b) Map of all atoms, both *Mn* and *Al,* in the same semi-supercluster as shown on the left inset in figure 5a. The difference represents the *Al* atoms. Notice that when the two outermost cluster layers (representing *Al* and *Mn*) merge—owing to limited phase-contrast microscope resolution—the clusters touch tangentially as in the experimental **Figure 6** below. Figures 5a and 5b together simulate figure 6 with convincing accuracy. Mapping scales are given in units of the measured quasi-lattice-parameter a [2].

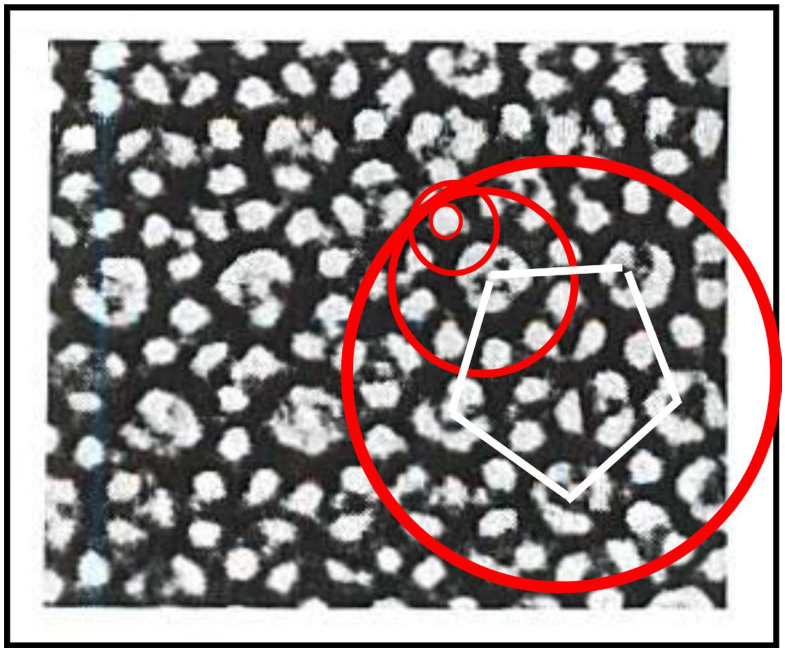

Figure 6. Hierarchic structure (red circles) on phase-contrast, optimum-defocus, transmission electron microscope image of Al_6Mn [19] [16] (p. 66), observed parallel to the 5-fold axis. The image shows hierarchic arrangement of M_n atoms (smallest circle) and (with increasing diameter) a unit cell (13 atoms), cluster (~12^2 atoms) and supercluster (~12^3 atoms). The centers of the clusters are located at the apices of the white pentagon. The structure is mapped in **Figure 5b**.

Their hypotenuse on (x_2,y_2) gives a radius that was plotted against z_0 in figures 5. Moreover, after calculating the heights of the projections, atoms within a given foil thickness were selected for display.

The simulated map of *Mn* atoms in one half of a supercluster, that is contained in a thin film about 2 nm thick, is shown in **Figure 5a** at left. The mapping calculation employs the same structure as is used for quasi structure factors [2] [4], except that Al atoms are ignored. The image shows the two 'circles' of M_n (**Figure 4**) that appear in 10-fold circles in the cluster; but only one 5-fold circle of clusters in the supercluster. By contrast, in the hierarchic semi-supercluster order 2, with a thickness of ~5 nm, the clusters appear to be 10-fold owing to the twin 'circles'. These features explain many characteristic structures in the phase contrast images [19].

Moreover, in transmission electron microscopy, optimum-phase-contrast sacrifices realism in image location because images change with defocus. Since the atomic scattering power of *Mn* is comparatively large, $f_{Mn}^2 \approx 4 \times f_{Al}^2$ [10], the skeleton *Mn* projections in the inset in **Figure 5a** should move toward 5b in a through focal series. Then, with typical loss of resolution, the skeleton will transform to the observed image in **Figure 6**. Here clusters touch tangentially as in a defocused projection of **Figure 5b**.

The mapping simulations match—both as patterns and by lateral measurements—the electron microscope image in **Figure 6**. They confirm the hierarchic concept[8], so that we can now proceed to discuss the most common defect structures.

[8]The maps dispel the common misconception that the structure is decagonal.

5. Elementary Defects

We begin by dividing the defects into 1) vacancies; or into 2) perfect interstitials without deformity; or 3) other defects, typically deformed. The second of these is significant because of the high density of the unit cell, that makes it the likely cause both for the driving force for the ideal icosahedral hierarchy, and for filling of intrinsic defects. There is evidence for this dominance of the unit cell in dynamic studies of QC growth [20] [21]. There, systematic realignment of atoms can be observed in unit cells and clusters that coalesce into superclusters and, presumably, into higher orders. It is obvious in the rearrangements, that the fundamental icosahedral orientation is maintained during the rearrangements. This must be the case where each cell shares two or more edges with its neighbors. The rigid orientation would occur to a greater or lesser extent if there were, during solidification, multiple nucleation sites, possibly of different sizes—atom, cell, cluster, etc. The coalescence is evident in growth and is surely significant in rapid cooling.

Because the structure is edge sharing, it gives the impression of being porous. Compared with typical crystals, the QC is slightly soft and viscous [22]. *The unit cell is extremely dense*, but higher orders contain "holes" (see Pauling's observation in [5]) especially at cluster and supercluster centers, but also on each side of shared edges. In higher orders, these spaces require filling. Guiding the study must be a concern for consistency in the icosahedral point group symmetry that reciprocates in the diffraction pattern. We will first consider vacancies and interstitials in the smallest structure, the unit cell (**Figure 3**), and proceed to clusters, and to superclusters in ascending hierarchic order (**Figure 4**). To ease comprehension, represent 3-dimensional icosahedra by corresponding 2-dimensional cross-sections: for the unit cell, that is the golden rectangle $\tau \times 1$ in **Figure 7**.

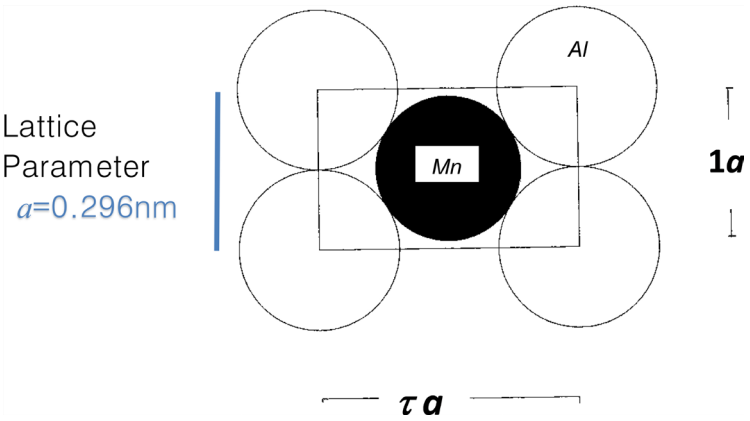

Figure 7. The cross-section above, that is taken from the unit cell shown in **Figure 3** is identical to the golden rectangles in **Figure 4**. The quasi-lattice-parameter a is measured as the edge width [2J. It is equal to the diameter of closely packed *Al*, $a = d_{Al}$. Notice that the diameter of the solute atom in this dense diatomic structure is given by $d_{\mathrm{Mn}} = \left(\sqrt{1+t^2} - 1\right)a$. The ratio $d_{\mathrm{solvent}}/d_{\mathrm{solute}}$ is universal in diatomic quasicrystals. Each unit cell has 15 identical sections at various orientations. The sections that will appear again in **Figure 8** are scaled versions of the section here.

This figure illustrates the dominating cross-section of the dense atomic model in Figure 3, including the unit cell and quasi-lattice parameter. The unit cell contains 15 identical cross-sections at different orientations. This orientational consistency can be thought of as roughly approximating cylindrical symmetry, with Euclidean axes. Because of edge sharing, various subsidiary spaces fill gaps on either side of the edges that join the dense unit cells. We simplify our understanding of the subsidiary cells by thinking of the 3-dimensional HI by its dominant 2-dimensional cross-section.

We can then consider in turn vacancies, perfect interstitials, and strained interstitials. These features can be made consistent with the sharp diffraction pattern by preserving icosahedral symmetry in all defects, or most of them. So in Figure 8,

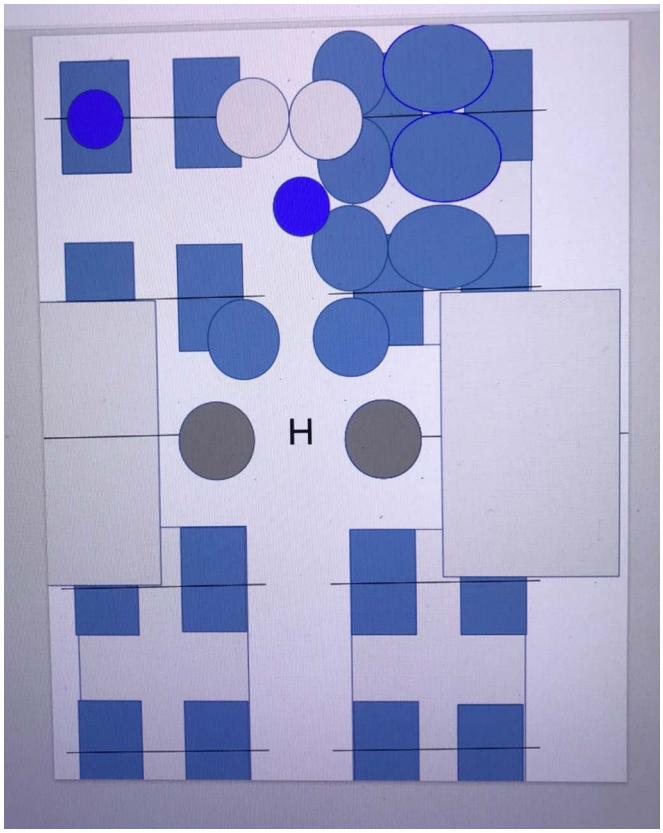

Figure 8. Hierarchic cross-section of a supercluster containing at its corners 4 cross-sections of clusters, each containing 4 rectangular cross-sections of *blue unit cells* (Figure 7). Blue circles represent *Al* atoms at corners of selected unit cells. The most elementary defects are considered: 1. *Vacancies* occur at *sites* that are closer spaced than the atomic diameters. The two 'mobile sites' (blue ellipses) may then be shared by one atom like an extended edge site, *e.g.* separated by $1/\tau$ at the top right corner cluster. 2. *Perfect interstitials*: *e.g.* the dark blue unit *Mn* atom (center top) between four clusters, occupying space—left open by the edge sharing clusters—without distortion. 3. *Off-plane* regular (hierarchic) structures (off white and dark grey) 4. *Other distorted interstitials* such as octagonal structures, not represented in the diagram. All of the critical dimensions in the figure belong to the geometric series τ^m, *e.g.* 1 for the diameter of the *Al* atom; $\tau \times 1$ for the rectangular unit cell (as in Figure 7, with units of *a*); $\tau^3 \times \tau^2$ for the cluster; $\tau^5 \times \tau^4$ for the supercluster; $1 \times \tau^{-1}$ for the cluster hole; $\tau^2 \times \tau$ for the supercluster hole H; *etc.*

icosahedra are represented by their 2-dimensional cross-sections: the unit cell, by the blue golden rectangle $\tau \times 1$; the cluster, by four unit cells $\tau^3 \times \tau^2$; the super-cluster, by four clusters $\tau^5 \times \tau^4$, *etc.*

In isolation, or in the melt before solidification, the *unit cell* is dense. However, when it is integrated into an hierarchic cluster, some sites are vacated because of insufficient space. We suppose that mobile *Al* atoms share neighboring sites that are closer together (separated by $1/\tau$) than the unit diameter of the atom. These mobile atoms are represented by elliptical wave functions on the *Al* atoms at corners of adjacent golden rectangles in the (top right) cluster in **Figure 8**. By contrast, typical the *Al* atoms are circular with unit (icosahedral) diameter. The vacancy is common at the cluster level in the hierarchy. For example, the central "hole" is icosahedral and may be represented, in cross-section, by the golden rectangle $1 \times 1/\tau$. It is so small that there is room for only three Al atoms on twelve ideal corner sites. These have been simulated [[4] p.54] in agreement with phase-contrast images.

The largest individual volume, at any tier of hierarchy, is the central "hole". In the supercluster it is marked with the letter H in **Figure 8**. This hole has the cross-section $\tau^2 \times \tau$. Its center is surrounded, in front and behind, by off-white cluster cross-sections, and closer in by *Al* atoms in dark grey. The "hole" is larger than the unit cell so there is more than one way in which the space can be filled. It could also be filled by an octahedral structure which may not show in diffraction because the octahedron is a subgroup of the icosahedral group.

An estimate can easily be calculated for the contribution to scattering caused by interstitial filling in the "hole". The supercluster has cross-section $\tau^5 \times \tau^4$; so that the volume of the "hole" is $\tau^{-6} \sim 5.6\%$ less voluminous. The same defect ratio holds for in-fill ratios at higher orders. This is why they can be neglected in first calculations but might be revealed in further detail by concerted research. Meanwhile, we have, for the most part, been able to leave the defect holes empty in QSF calculations, since the effects of their tentative, possible inclusions were small. In this paper, primacy is given to logarithmic periodicity, hierarchic structure and resonant response; details of the structural "jig-saw puzzle"—what we here call defects—are relegated, because their effects are comparatively small and insignificant.

6. Conclusions

Whatever may be the structural details of quasicrystals, whether systematic or accidental; the ideal hierarchic model has provided complete understanding of diffraction in geometric series with irrational indices. Quasicrystals have demonstrated that quantum physics and Bragg diffraction are not beautiful mathematics but empirical physics: the proof of the numeric metric by analytic separation of the irrational residue is a benefit of observation over speculative expectation. The coherent scattering, that is here described, depends on constructive interference—in time and space—of the incident radiation. We have shown how

logarithmically-periodic solids digitize and harmonize incident periodic waves. The radiation responds to the hierarchic QC fields by forming quasi-Bloch waves on a special *metric*. This formation commensurates the periodic, incident radiation with the varied and irrationally-spaced, hierarchic quasicrystal. Quasi-structure factors show that the resulting translational periodicity about $a\tau^m$, scatters the radiation coherently into geometric reciprocal space. There *is* long range order and this is evident in the diffraction. However, the corresponding *translational symmetry occurs by resonant response of the scattering radiation.* Without harmonics, the scattering would be random owing to destructive interference within the wave packet. Spectacularly, this doesn't happen.

Moreover, in this work, we have united time-dependent wave optics in 4-dimensions (Section 2) with more typical 3-dimensional optics that is adapted from Bragg optics. The time dependence is necessary to show how the quantum effects—evident in both atomic states and in diffraction—occur by harmonies, in the physical domain, and are commonly glossed in purely mathematical descriptions. The harmonics are furthermore associated with QC defects that are represented, for easy comprehension, by 2-dimensional cross-sections. These are scaled for the various hierarchies. Based, as they are, on the exact description of the diffraction, the present physical description of harmonic quanta, has wider application in general physics.

Conflicts of Interest

The author declares no conflicts of interest regarding the publication of this paper.

References

[1] Shechtman, D., Blech, I., Gratias, D. and Cahn, J.W. (1984) *Physical Review Letters*, **53**, 1951-1953. https://doi.org/10.1103/PhysRevLett.53.1951

[2] Bourdillon, A.J. (2020) *Journal of Modern Physics*, **11**, 581-592. https://doi.org/10.4236/jmp.2020.114038

[3] Bourdillon, A.J. (2020) Quasicrystal Bloch Wave Symmetry about at^m. https://www.youtube.com/watch?v=gZClVNKhhVw

[4] Bourdillon, A.J. (2011) Logarithmically Periodic Solids. Nova Science, Hauppauge.

[5] Pauling, L. (1985) *Nature*, **317**, 512-514. https://doi.org/10.1038/317512a0

[6] Bourdillon, A.J. (2017) Dispersion Dynamics in the Hall Effect and Pair Bonding in HiT_c. Nova Science, Hauppauge.

[7] Dirac, P.A.M. (1958) The Principles of Quantum Mechanics. Oxford University Press, Oxford. https://doi.org/10.1063/1.3062610

[8] Feynman, R.P. (1949) *Physical Review*, **76**, 749-769. https://doi.org/10.1103/PhysRev.76.769

[9] Stueckelberg, E.C.G. (1941) *Helvetica Physics Acta*, **14**, 588-594.

[10] Hirsch, P., Howie, A., Nicholson, R.B., Pashley, D.W. and Whelan, M.J. (1977) Electron Microscopy of Thin Crystals. Krieger, New York.

[11] Bourdillon, A.J. (2010) Quasicrystals' 2D Tiles in 3D Superclusters. UHRL, San Jose,

p. 37 *seq*.

[12] Bourdillon, A.J. (2018) *Journal of Modern Physics*, **9**, 1304-1316. https://doi.org/10.4236/jmp.2018.96079

[13] Bourdillon, A.J. (2018) *Journal of Modern Physics*, **9**, 2295-2307. https://doi.org/10.4236/jmp.2018.913145

[14] Bourdillon, A.J. (2020) *Journal of Modern Physics*, **11**, 1926-1937. https://doi.org/10.4236/jmp.2020.1112121

[15] Bourdillon, A.J. (2019) *Journal of Modern Physics*, **10**, 624-634. https://doi.org/10.4236/jmp.2019.106044

[16] Bourdillon, A.J. (2009) Quasicrystals and Quasi Drivers.

[17] Bourdillon, A.J. (2009) *Solid State Communications*, **149**, 1221-1225. https://doi.org/10.1016/j.ssc.2009.04.032

[18] Bourdillon, A.J. (2013) *Micron*, **51**, 21-25. https://doi.org/10.1016/j.micron.2013.06.004

[19] Bursill, L.A. and Peng, J.L. (1985) *Nature*, **316**, 50-51. https://doi.org/10.1038/316050a0

[20] Nagao, K., Inuzuka, T., Nishimoto, K. and Edagawa, K. (2015) *Physical Review Letters*, **115**, Article ID: 075501. https://doi.org/10.1103/PhysRevLett.115.075501

[21] Thi, N.H., Gastaldi, J., Schenk, T., Reinhart, G., Mangelinck-Noel, N., Cristiglio, V., Billia, B., Grushko, B., Hartwig, J., Klein, H. and Baruchel, J. (2006) *Physical Review E*, **74**, Article ID: 021605. https://doi.org/10.1103/PhysRevE.74.031605

[22] Puckerman, B.E. (2011) Quasicrystals: Types, Systems, and Techniques. Nova Science, Hauppauge.